No. 582 **February 2018**

An Investigation on Separation Points of Power-Law model Along a Rotating Round-Nosed Body

N. Begum, S. Siddiqa, A. Ouazzi, Md. A. Hossain

ISSN: 2190-1767

An Investigation on Separation Points of Power-Law model Along a Rotating Round-Nosed Body

Naheed Begum[§], Sadia Siddiqa[*,1], A. Ouazzi[§], Md. Anwar Hossain[‡]

[§]*Institute of Applied Mathematics (LSIII), TU Dortmund, Vogelpothsweg 87, D-44227 Dortmund, Germany*

[*]*Department of Mathematics, COMSATS Institute of Information Technology, Kamra Road, Attock, Pakistan*

[‡]*UGC Professor, University of Dhaka, Dhaka, Bangladesh*

Abstract: The purpose of present study is to numerically investigate the natural convection flow of Ostwalde-de Waele type power law non-Newtonian fluid along the surface of rotating axi-symmetric round-nosed body. For computational purpose rotating hemisphere is used as a case study in order to examine the heat transfer mechanism near such transverse curvature geometries. The numerical scheme is applied after converting the dimensionless system of equations into primitive variable formulations. Implicit finite difference method is used to integrate the equations numerically. Its worth mentioning that all the numerical simulations performed here are valid particularly for the class of shear thickening fluid with wide range of Prandtl number, i.e. $(10.0 \leq \mathrm{Pr} \leq 1500.0)$. A detailed discussion is done to understand the effects of buoyant forces and power-law exponents on the rate of heat transfer and skin friction coefficient at the surface of the hemisphere. Comparison of present numerical results for different values of buoyancy ratio parameter λ with other published data has been shown in graphical form. For the first time the velocity profiles are plotted at the point of separation, which occurs when the portion of the boundary layer closest to the wall or leading edge reverses in flow direction. It is recorded that an increase in the power-law index n and Prandtl number Pr leads to an increase in the friction factor as well as in the rate of heat transfer.

Keywords: Modified Power-Law, Non-Newtonian Fluid, Natural Convection, Round-nosed Bodies.

1 Introduction

In the past decades, the flows occurred due to axi-symmetric round nosed bodies has attracted many experimentalists and investigators because of their applications in optimization industries of the flying vehicles. For instance, such "blunt" round-nosed shapes can be visualized on large aircraft and on subsonic vehicles. Numerous commercial aircrafts that fly at subsonic speed are idealistically designed to adopt the shape as parabolic (rounded) nose. The main influence of nose blunting has been recorded to be the minimization of drag factor, for certain levels of rounding radius, compared with the corresponding sharp nosed body flow. In addition, cones and rotating spheres are deliberately hired as nose cones in many spinning projectile applications and aeroengine. Suwono [1] was the first to study the effects of buoyant-forces on boundary layer flow of viscous flow along rotating axi-symmetric round-nosed bodies. In [1], a detailed theoretical analysis is presented to study the heat

[1]Corresponding author.
Email: saadiasiddiqa@gmail.com

transfer mechanism for the case of rotating hemisphere. The author used G*ö*ortler series expansion method for numerical solution of boundary layer problem for different values of buoyancy ratio parameter $\lambda = Gr/Re^2$ ranging between 0 to ∞ with Prandtl number $0.72 < \mathrm{Pr} < 100$. From the numerical results, the authors concluded that the buoyancy is more influential for flows generated by rotating bodies than the flows over submerged bodies. Later Hossain *et al.* [2]-[3] investigated the boundary layer problem near rotating hemisphere shaped round nosed bodies with the aid of local non-similarity method and Keller-box method. Recently, Siddiqa *et al.* [4] studied an interesting problem of two-phase natural convection dusty fluid flow past a rotating axi-symmetric round-nosed body. In [4], the authors employed implicit finite difference method to obtain the solutions of two-phase problem and concluded that buoyancy forces emerged from rotating hemisphere are a major factor to enhance the heat transport rate near the leading edge.

In all the above references, the authors focused only on Newtonian fluid flows. But, many practical applications involve the fluids having complex nature. For instance, most of the particulate slurries such as coal in water, synthetic lubricants, polymers, paints, emulsions, biological fluids such as blood, food stuffs such as marmalades, jellies and jams are few examples of fluids having non-Newtonian nature. Therefore, the characteristics of non-Newtonian fluid flow is important in many application of practical interest. Couple stress fluids, micropolar fluids, visco-elastic fluids and power-law fluids are a few of many fluids having non-Newtonian attributes. Although, several constitutive laws have been established to describe the behavior of non-Newtonian fluids, but the most deliberately used model in non-Newtonian fluid mechanics is the Ostwald-de Waele type power-law model (for details see [5]):

$$\tau_{ij} = -p\delta_{ij} + K\left|\sum_{m=1}^{3}\sum_{l=1}^{3} e_{lm}e_{lm}\right|^{(n-1)/2} e_{ij} \tag{1}$$

where p, δ_{ij}, K, n, respectively, denotes the pressure, Kronecker delta, consistency coefficient and power-law index of the fluid. It is important to mention here that: i) $n < 1$ represents the class of pseudo-plastic fluids (shear thinning), ii) $n > 1$ corresponds to dilatant fluids (shear thickening) and iii) $n = 1$ are simply the Newtonian type fluids. An extensive research in the past reveals the fact that the range $0.0 < n \leq 2.0$ is valid for the power-law index n. Numerous researchers and analysts studied heat and mass transfer problems by taking into account such non-Newtonian fluids. In this regard, Schowalter [6] investigated the two- and three-dimensional boundary-layer problem for pseudoplastic non-Newtonian fluids which can be characterized by a power-law relationship between shear stress and velocity gradient. Acrivos [7] performed the theoretical analysis of laminar natural convection heat transfer to non-Newtonian fluids and introduced the similarity variables for general wedge flow of power-law fluids. In this paper, the author proved that how the well-established expressions for the rate of heat transfer of Newtonian fluids may be generalized to include the non-Newtonian effects. Lee and Ames [8] discussed the similarity equations and solutions for various non-Newtonian viscoinelastic fluids under right wedge geometry. A complete survey of the literature on non-Newtonian fluids is impractical; however, a few items are listed here to provide the initial investigations for a broader literature (for details see Refs. [9]-[13]). In later years, Kawase and Ulbrecht [14] presented the approximate solutions for the problem of heat transfer free convective flow along a vertical wall. Afterwards, Huang *et al.* [15] reported the influence of Prandtl number on free convection flow of power-law non-

Newtonian fluids from a vertical plate. In [15], the authors presented similarity solutions and concluded that the average heat transport rate is promoted owing to an increase in Prandtl number. Later on, Kumari *et al.* [16] presented a theoretical analysis for free convective laminar boundary-layer flow of non-Newtonian power-law fluid. In this paper, the authors exploited a vertical sinusoidal wavy geometry and established the numerical solutions via Keller-Box method for wide range of Prandtl number. Subsequently, a large amount of work for non-Newtonian fluids including integral, experimental, and numerical methods, was presented under different physical circumstances (see Refs. [17]-[21]).
To the best of author's knowledge, the problem of non-Newtonian power-law fluid flow along the transverse round-nosed bodies is not investigated so far. Thus, the present work has been undertaken to give the more detailed analysis of boundary layer flow of non-Newtonian fluid with the interaction of blunt bodies. Primitive variable formulation (PVF) is employed for transforming the set of boundary layer equations of non-Newtonian fluid flow into a convenient system. Numerical solutions for the underlying coupled, nonlinear system is then obtained with the aid of two-point finite difference method together with the Thomas Algorithm. The effects of transverse curvature geometry and non-Newtonian nature of the fluid on flow and heat transfer characteristics are examined and discussed in detail. For the full demonstration of the various non-Newtonian fluids, the behaviors of both Newtonian and dilatant fluids on the natural convection laminar flow along an isothermally heated round nosed body is studied by choosing the power-law index as ($1.0 \leq n \leq 2.0$).

2 Problem Formulation

The physical model considered here is laminar boundary layer flow of power-law fluid along a rotating round-nosed body with constant surface temperature, T_w, such that $T_w >> T_\infty$, where T_∞ is undisturbed temperature of ambient non-Newtonian fluid. In our detailed computational work, the kinematic viscosity ν depends on shear-rate and is correlated by a modified power-law. The Boussinesq approximation is considered to be valid in this analysis. The schematic representation of co-ordinate system is given in Fig. 1. By taking into account above-mentioned assumptions, the governing equations for the non-Newtonian, steady, incompressible fluid flow can be written in the underlying form:

$$\frac{\partial \bar{u}}{\partial \bar{x}} + \frac{\partial \bar{v}}{\partial \bar{y}} + \frac{\bar{u}}{\bar{r}}\frac{d\bar{r}}{d\bar{x}} = 0 \tag{2}$$

$$\bar{u}\frac{\partial \bar{u}}{\partial \bar{x}} + \bar{v}\frac{\partial \bar{u}}{\partial \bar{y}} - \frac{\bar{w^2}}{\bar{r}}\frac{d\bar{r}}{d\bar{x}} = \frac{\partial}{\partial \bar{y}}\left(\nu\frac{\partial \bar{u}}{\partial \bar{y}}\right) + g\beta\left(T - T_\infty\right) \tag{3}$$

$$\bar{u}\frac{\partial \bar{w}}{\partial \bar{x}} + \bar{v}\frac{\partial \bar{w}}{\partial \bar{y}} + \frac{\bar{u}\bar{w}}{\bar{r}}\frac{d\bar{r}}{d\bar{x}} = \frac{\partial}{\partial \bar{y}}\left(\nu\frac{\partial \bar{w}}{\partial \bar{y}}\right) \tag{4}$$

$$\bar{u}\frac{\partial T}{\partial \bar{x}} + \bar{v}\frac{\partial T}{\partial \bar{y}} = \frac{\kappa}{\rho c_p}\frac{\partial^2 T}{\partial \bar{y}^2} \tag{5}$$

where T, c_p, ρ, g, β and κ are respectively represents the temperature, specific heat at constant pressure, density, gravitational acceleration, volumetric expansion coefficient and thermal conductivity. In present scenario, $(\bar{x}, \bar{y}, \bar{z})$ are the curvilinear coordinates, $\bar{u}$ is the velocity component in the direction of surface-contour, $\bar{v}$ the velocity component in the normal direction and $\bar{w}$ the tangential velocity component in rotating $\bar{z}$ direction. In boundary

layer fluid flows, the viscosity ν of non-Newtonian fluids may often be characterized with satisfactory accuracy by modified power-law (see Ref. [5]), which is:

$$\nu = \frac{K}{\rho}\left|\frac{\partial \bar{u}}{\partial \bar{y}}\right|^{n-1} \tag{6}$$

where, K is a dimensional empirical constant, the dimension of which depends on the power-law index n. The fundamental equations stated above are to be solved under appropriate boundary conditions to determine the flow fields. The boundary conditions to be satisfied are:

$$\begin{aligned} &\bar{u} = \bar{v} = 0, \quad \bar{w} = \bar{r}\Omega, \quad T = T_w \quad \text{at} \quad \bar{y} = 0 \\ &\bar{u} \to 0, \quad \bar{w} \to 0, \quad T \to T_\infty \quad \text{as} \quad \bar{y} \to \infty \end{aligned} \tag{7}$$

By introducing a reference length L and a reference velocity $U_c = L\Omega$, we establish dimensionless dependent and independent variables according to the following continuous transformations:

$$\begin{aligned} &x = \frac{\bar{x}}{L}, \quad r = \frac{\bar{r}}{L}, \quad y = \frac{\bar{y}}{L} Re^{\frac{1}{2(n+1)}}, \quad u = \frac{\bar{u}}{U_c}, \quad v = \frac{\bar{v}}{U_c} Re^{\frac{1}{2(n+1)}}, \quad w = \frac{\bar{w}}{U_c}, \\ &\Delta T = T_w - T_\infty, \quad \theta = \frac{T - T_\infty}{\Delta T}, \quad Gr = \frac{g_x \beta \Delta T L^{4n+1}}{U_c^{4n-6}(K/\rho)^4}, \quad Re = \frac{L^{2n}}{U_c^{2n-4}(K/\rho)^2}, \\ &\Pr = \frac{1}{\alpha}\left(\frac{K}{\rho}\right)^{2/(1+n)} L^{\frac{(1-n)}{(1+n)}} U_c^{\frac{3(n-1)}{(n+1)}}, \quad \lambda = \frac{Gr}{Re^2} \end{aligned} \tag{8}$$

where λ, Gr, Re and Pr are the buoyancy ratio parameter, generalized Grashof number, Reynolds number and Prandtl number, respectively. The acceleration due to gravity for the round-nosed geometry is defined as $g = g_x A(x)$, where $A(x)$ is dimensionless function of x. Now, by incorporating the transformations in (8) into the above system of governing Eqs. (2)-(7), we will obtain the following system of equations:

$$\frac{\partial u}{\partial x} + \frac{\partial v}{\partial y} + \frac{u}{r}\frac{dr}{dx} = 0 \tag{9}$$

$$u\frac{\partial u}{\partial x} + v\frac{\partial u}{\partial y} - \frac{w^2}{r}\frac{dr}{dx} = \frac{\partial}{\partial y}\left(\left|\frac{\partial u}{\partial y}\right|^{n-1}\frac{\partial u}{\partial y}\right) + \lambda A(x)\theta \tag{10}$$

$$u\frac{\partial w}{\partial x} + v\frac{\partial w}{\partial y} + \frac{uw}{r}\frac{dr}{dx} = \frac{\partial}{\partial y}\left(\left|\frac{\partial u}{\partial y}\right|^{n-1}\frac{\partial w}{\partial y}\right) \tag{11}$$

$$u\frac{\partial \theta}{\partial x} + v\frac{\partial \theta}{\partial y} = \frac{1}{\Pr}\frac{\partial^2 \theta}{\partial y^2} \tag{12}$$

The transformed boundary conditions are:

$$\begin{aligned} &u = v = 0, \quad w = r, \quad \theta = 1 \quad \text{at} \quad y = 0, \\ &u \to 0, \quad w \to 0, \quad \theta \to 0 \quad \text{as} \quad y \to \infty, \end{aligned} \tag{13}$$

Before employing the numerical scheme, the system of equations is converted into convenient form with the aid of primitive variable formulations. For this we define the following set of

continuous transformations:

$$\begin{aligned} &u = rU, \quad v = r^2 \left(2X\right)^{\frac{-1}{(n+1)}} V, \quad w = rW, \quad \theta = \Theta, \\ &X = \int_0^x r^3 d\left(x\right), \quad Y = r^2 \left(2X\right)^{\frac{-n}{(n+1)}} y. \end{aligned} \tag{14}$$

The transformed equations are:

$$2P\left(x\right)U + 2I(x)\frac{\partial U}{\partial x} + \left(2P\left(x\right) - \frac{2n}{n+1}\right) Y \frac{\partial U}{\partial Y} + \frac{\partial V}{\partial Y} = 0 \tag{15}$$

$$\begin{aligned} 2UI(x)\frac{\partial U}{\partial x} + \left(V + \left(2P\left(x\right) - \frac{2n}{n+1}\right) UY\right) \frac{\partial U}{\partial Y} + P\left(x\right)\left(U^2 - W^2\right) \\ = R\left(x\right) \frac{\partial}{\partial Y} \left(\left|\frac{\partial U}{\partial Y}\right|^{n-1} \frac{\partial U}{\partial Y}\right) + \lambda Q\left(x\right)\Theta \end{aligned} \tag{16}$$

$$\begin{aligned} 2UI(x)\frac{\partial W}{\partial x} + \left(V + \left(2P\left(x\right) - \frac{2n}{n+1}\right) UY\right) \frac{\partial W}{\partial Y} + 2P\left(x\right)UW \\ = R\left(x\right) \frac{\partial}{\partial Y} \left(\left|\frac{\partial W}{\partial Y}\right|^{n-1} \frac{\partial W}{\partial Y}\right) \end{aligned} \tag{17}$$

$$2UI(x)\frac{\partial \Theta}{\partial x} + \left(V + \left(2P\left(x\right) - \frac{2n}{n+1}\right) UY\right) \frac{\partial \Theta}{\partial Y} = \frac{(2X)^{(1-n)/(n+1)}}{\mathrm{Pr}} \frac{\partial^2 \Theta}{\partial Y^2} \tag{18}$$

subject to the boundary conditions:

$$\begin{aligned} U(X,0) = V(X,0) = 0, \quad W(X,0) = \Theta(X,0) = 1, \\ U(X,\infty) = W(X,\infty) = \Theta(X,\infty) = 0 \end{aligned} \tag{19}$$

It is noteworthy to mention here that axi-symmetric bodies with rounded shapes are of prime interest because of the physical reason that i) they have been considered an essential component for adequate radar installation and (ii) to derive optimum shapes mathematically that have a minor blunt area at the tip. As far as present analysis is concerned, we will focus our attention on the application of results which are related with rotating hemisphere with radius $\bar{R}$. If we set R (oriented parallel with respect to the g) to be characteristic reference length, *i.e.*, $\bar{R} = L$, then the underlying non-dimensional variables can be obtained:

$$r(x) = A(x) = \sin x, \quad X = \frac{1}{3}(\cos^3 x - 3\cos x + 2) \tag{20}$$

Therefore for the case of hemisphere, the values of $P(x)$, $Q(x)$, $R(x)$ and $I(x)$ are evaluated as follows:

$$\begin{aligned} P(x) = \frac{2\cos x(\cos^3 x - 3\cos x + 2)}{3\sin^4 x}, \quad Q(x) = \frac{2(\cos^3 x - 3\cos x + 2)}{3\sin^4 x}, \\ R(x) = (\sin x)^{3n-3} \left(\frac{2(\cos^3 x - 3\cos x + 2)}{3}\right)^{-n+1}, \quad I(x) = \frac{(\cos^3 x - 3\cos x + 2)}{3\sin^3 x} \end{aligned} \tag{21}$$

The interaction among the continuity, momentum and energy equations for non-Newtonian fluid, given in Eqs. (15)-(19), are solved numerically by hiring two-point implicit finite difference method together with Thomas algorithm. The central difference is used for the

diffusion terms and the forward difference scheme is used for the convection terms. The singularity at $X = 0$ has been removed by the scaling, therefore, the computation can be started at $X = 0.0$, and then marches downstream implicitly along with the boundary layer regime. For a given value of X, the iterative procedure is stopped when the difference of the previous and the present iteration, while computing the velocity and the temperature, is less than 10^{-6}. The details regrading the discretization procedure and numerical scheme is given in [22].

As the physical quantities, skin friction coefficient and Nusselt number, are of remarkable importance both experimentally and scientifically, therefore, solutions are expressed in terms of them once we know the values of the unknowns. The expressions of the skin-friction coefficient, C_f, and rate of heat transfer Nu can be calculated from the following relations:

$$\begin{aligned} \tau = C_f Re_0 Re^{\frac{2n+1}{2(n+1)}} &= (2X)^{-n/(n+1)}\, r^3 \left(\frac{\partial U}{\partial Y}\right)_{Y=0}, \\ Q = NuRe^{\frac{-1}{2(n+1)}} &= -(2X)^{-n/(n+1)}\, r^2 \left(\frac{\partial \Theta}{\partial Y}\right)_{Y=0} \end{aligned} \tag{22}$$

The numerical results are discussed in the upcoming section of the manuscript.

3 Results and Discussion

The prime purpose of present analysis is to report the effects of buoyancy parameter λ on boundary layer flow of non-Newtonian fluid along a rotating axi-symmetric round nosed body having hemisphere configurations. In this work, the influence of non-Newtonian nature of fluid is elucidated with the aid of modified power-law viscosity model. The detailed simulations are performed for non-linear coupled mathematical system given in Eqs. (15)-(19) by employing the implicit finite difference method. In order to gain some understanding of this non-Newtonian power-law fluid flow problem along a transverse geometry of hemisphere, the influence of important parameters on the distribution of rate of heat transfer, shear stress and velocity profiles are graphed and discussed. Particularly, the main point of interest is to visualize the separation of fluid from the surface, which is caused due to the variation of buoyancy parameter, λ, and power-law index, n, and Prandtl number Pr in stream-wise direction X.

For verification of accuracy of results and numerical scheme, graphical comparison is presented with already published data for the class of Newtonian fluid by setting $n = 1.0$. It is noteworthy to mention here that the work of Suwono [1] and Hossain *et al.* [3] can be retrieved and become special cases of our study for $n = 1.0$. In [1], computational results are obtained by using Runge-Kutta-Merson (RKM) method, near the leading edge when axial coordinate is taken very small. While in the analysis of Hossain *et al.* [3], Keller box method is hired to perform the simulations for the whole range of axial coordinate. Our computational results are also obtained for the same range of axial coordinate X, from the two-point implicit finite difference method. In-spite of using different methods and formulations as well, the results for skin friction coefficient and rate of heat transfer are obtained and compared graphically in Fig. 2 by setting the parameters as: Pr $= 0.72$, $\lambda = 0.1, 0.5, 1.0$, and $n = 1.0$. From Fig. 2, it can be concluded that the solutions produced

through finite difference method are in a good agreement with those obtained from RKM (see [1]) and Keller box method (see [3]).

Figure 3 presents the variation in τ and Q by varying the values of buoyancy ratio parameter, λ, for the flow of dilatant non-Newtonian fluid with power-index $n = 1.6$ past a hemisphere. The contribution of buoyancy ratio parameter on the physical quantities is presented for three different cases, *i.e.* i) $\lambda < 0.0$ with opposing buoyancy flow, ii) $\lambda = 0.0$ for purely forced convective flow and iii) $\lambda > 0.0$ with assisting buoyancy flow. For present scenario, it is observed that both τ and Q tends to increase by increasing the values of parameter λ from -0.2 to 5.0 for non-Newtonian fluid characterized by sufficiently large value of Prandtl number. Particularly, such influence of increasing values of λ is more influential for drag coefficient at the surface of hemisphere. The reason for such trend is that $\lambda > 0.0$ accelerates the fluid flow and acts a retarding factor for the thickness of momentum boundary layer and consequently τ increases (see Fig. 3(a)). Such magnifying contribution of buoyancy ratio parameter has also been observed for rate of heat transfer coefficient in Fig. 3(b), but not as much strong as in case of skin friction coefficient. Mathematically, the reason for comparatively weaker dependence of Q on λ is that the buoyancy parameter does not have an explicit occurrence in the temperature equation (see Eq. (18)).

Figure 4 display the influence of different values of Prandtl number on the distribution of skin friction coefficient, τ and rate of heat transfer Q. The results are presented for wide range of Prandtl number Pr starting from 10.0 to 1500.0. For comparison purpose, physical quantities are plotted for Newtonian as well as for non-Newtonian fluid of shear thickening nature. It can be observed from Fig. 4(a) that the skin friction coefficient decreases sufficiently owing to an increase in the values of Pr from 10.0 to 1500.0. Specifically, the retarding effect of large values of Pr is more dominant for the class of dilatant fluids, *i.e.* for $n >> 1.0$. In addition, it is also interesting to observe that the shear thickening fluids show more resistance to flow than the fluids with Newtonian behavior for all values of Prandtl number Pr. Such behavior of skin friction coefficient is quite expected due to the fact that the dilatant fluids ($n >> 1.0$) are more viscous in nature than the Newtonian ones ($n = 1.0$). Therefore, the viscous effects get stronger for large values of n, which is responsible to produce more frictional forces and ultimately the skin friction coefficient, τ, tends to increase in the vicinity of rotating hemisphere. In addition, Fig. 4(b) reveals the fact that the rate of heat transfer, Q exhibits the tendency to increase by magnifying both Pr and n. More importantly, the shear thickening fluids ($n >> 1.0$) have large values of rate of heat transfer as compared to Newtonian fluids ($n = 1.0$) specially for $\Pr >> 100.0$.

For the first time, velocity profiles of shear thickening fluids for the underlying geometry are obtained at the point of separation. In Fig. 5 distributions are given for various values of n. It is observed that momentum boundary layer decreases when power-law index increases from 1.2 to 1.4. It is important to note that the peak of the velocity distributions come towards the origin, which means that separation point moves near to the origin for increasing n. Therefore, power-law index is one of the factor that causes the separation to occur earlier. The particular points of separation (x_s) and their corresponding values of velocity gradient for $n = 1.2 - 1.4$ are given in Table 1.

Velocity profiles of shear thickening fluid for opposing buoyancy flow under the effect of Prandtl number Pr is displayed in Fig. 6. These velocity profiles are also plotted at the point of separation. The behavior of velocity distributions ensure that the separation occurs almost at the same point for all values of Pr. In physical context, Pr is an important

Table 1: Points of separation for different values of power-law index n

$n = 1.2$		$n = 1.3$		$n = 1.4$	
x_s	τ	x_s	τ	x_s	τ
1.49100	-0.0469	1.49100	-0.00912	1.49400	-0.15816

parameter in heat transport phenomenons as it controls the relative thickness of momentum and thermal boundary layers. It can be clearly seen from Fig. 6 that the peaks of fluid velocity becomes higher by increasing the value of Pr from 400.0 to 1000.0. Thus, sufficiently large values of Pr acts like a driving force that increases the velocity of shear thickening fluid within the boundary layer region. It is also interesting to see that the dilatant fluid quickly attains the asymptotic behavior in the momentum boundary layer region for Pr $>$ 500.0. For different values of Pr, the particular points of separation (x_s) and their corresponding values of velocity gradient are given in Table 2.

Table 2: Points of separation for different values of Prandtl number Pr

Pr=400		Pr=600		Pr=1000	
x_s	τ	x_s	τ	x_s	τ
1.44600	-0.03709	1.47900	-0.10149	1.49100	-0.0469

Figure 7 is plotted to see the influence of buoyancy ratio parameter, λ, on the distribution of velocity profiles of dilatant fluid along a hemisphere. Physically, the effects of buoyant-forces on the flow due to rotating axi-symmetric bodies with constant surface temperature are of great importance as they also influence the shear thickening nature of fluids. As mentioned earlier, the dilatant fluid exhibits a tendency to get separate from the transverse geometry of hemisphere for negative values of buoyancy ratio parameter λ, therefore, Fig. 7 is plotted to see the distribution of velocity at the point of separation. It can be noted that by increasing λ from -1.0 to -0.6, the velocity distribution inside the boundary layer tends to reduce and its peak moves away from the leading edge. Thus, large values of λ acts as a delays the separation point and keep the local flow attached for as long as possible, which is important from engineering point of view. The points of separation (x_s) and their corresponding values of velocity gradient are given in Table 3 for various values of λ.

Table 3: Points of separation for different values of buoyancy ratio parameter, λ

$\lambda = -1.0$		$\lambda = -0.8$		$\lambda = -0.6$	
x_s	τ	x_s	τ	x_s	τ
1.31401	-0.01224	1.37401	-0.09944	1.43400	-0.00008

4 Conclusion

The present analysis aims to compute the numerical results of boundary layer flow of non-Newtonian power law fluid along an axi-symmetric round nosed bodies. Numerical solutions of the equations, governing the flow, are obtained by the use of an implicit finite difference method. In order to incorporate the non-Newtonian fluid into the analysis, modified viscosity model is employed. Numerical results give a clear insight towards understanding the response of the transverse curvature of the surface. The influence of emerging parameters is explored by expressing their relevance on skin friction coefficient and rate of heat transfer. Most importantly, velocity distributions are plotted at the point of separation for dilatant type of non-Newtonian fluids. The agreement of our numerical results with [1], [3] are found excellent. It is recorded that the rate of heat transfer for Newtonian fluids ($n = 1.0$) is less as compared to shear thickening fluids ($n > 1$), while on the other hand, large values of Prandtl number Pr and power-law exponent n contributes significantly to increase the rate of heat transfer. This piece of work finds numerous practical applications in manufacturing of foods, petroleum drilling and in production of slurries and polymers. Particularly, the concept of non-Newtonian power-law fluid in boundary layer has application in the reduction of frictional drags in many engineering process.

References

[1] Suwono, A., Buoyancy effects on flow and heat transfer on rotating axi-symmetric round-nosed bodies, *Int. J. Heat Mass Transfer*, **23**, 1980, 819-831.

[2] Hossain, M. A., Das, S. K., Pop, I., MHD free convection flow near rotating axi-symmetric round-nosed bodies, *Magnitnaya Gidrodinamika*, **2**, 1996, 68-73.

[3] Hossain, M. A., Anghel, A., Pop, I., Thermal radiation effects on free convection over a rotating axi-symmetric body with application to rotating hemispehere, *Arch. Mech.*, **54**, 2002, 55-74.

[4] Siddiqa, S., Begum, N., Hossain, M. A., Gorla, R. S. R., Two-Phase dusty fluid flow along a rotating axisymmetric round-nosed body, *ASME Journal of Heat Transfer*, **139**, 2017.

[5] Ostwald, W., Ueber die rechnerische Darstellung des Strukturgebietes der Viskositt, *Kolloid Z.*, **47**, 1929, 176187.

[6] Schowalter, W. R., The application of boundary layer theory to power law pseudo-plastic fluids, *AIChE J.*, **6**, 1960, 24-28.

[7] Acrivos, A., A theoretical analysis of laminar natural convection heat transfer to non-Newtonian fluids, *AIChE J.*, **16**, 1960, 584-590.

[8] Lee, S. Y., Ames, W. F., Similarity solutions for non-Newtonian fluids, *AIChE.*, **12**, 1966, 700-708.

[9] Na, T. Y., Hansen, A. G., Possible similarity solutions of the laminar natural convection flow of non-Newtonian fluids, *Int. J. Heat Mass Transf.*, **9**, 1966, 261-262.

[10] EDE, A. J., Advances in free convection, *Advances in Heat Transf.*, **4**, 1967, 1-64, Academic, New York.

[11] Sharma, K. K., Adelman, M., Experimental study of natural convection heat transfer from a vertical plate in a non-Newtonian fluid, *Can. J. Chem. Eng.*, **47**, 1969, 553-555.

[12] Dale, J. D., Emery, A. F., The free convection of heat from a vertical plate to several non-Newtonian pseudoplastic fluids, *J. Heat Transf.*, **94**, 1972, 64-72.

[13] Chen, T. V. W., Wollersheim, D. E., Free convection at a vertical plate with uniform flux condition in non-Newtonian power-law fluids, *J. Heat Transf.*, **95**, 1973, 123-124.

[14] Kawase, K., Ulbrecht, J., Approximate solution to the natural convection heat transfer from a vertical plate, *Int. Commun. Heat Mass Transf.*, **11**, 1984, 143-155.

[15] Huang, M. J., Huang, J. S., Chou, Y. L., Chen, C. K., Effects of Prandtl number on free-convection heat transfer from a vertical plate to a non-Newtonian fluid, *J. Heat Transf.*, **111**, 1989, 189-191.

[16] Kumari, M., Pop, I., Takhar, H. S., Free convection boundary layer flow of a non-Newtonian fluid along a vertical wavy surface, *Int. J. Heat and Fluid Flow*, **18**, 1997, 625-631.

[17] Pop, I. Gorla, R. S. R., Mixed convection similarity solutions of a non-Newtonian fluid on a horizontal surface, *J. Heat Mass Transf.*, **33**, 1991, 57-63.

[18] Wang, T. Y., Mixed convention heat transfer from a vertical plate to non-Newtonian Fluids, *Int. Commun. Heat Mass Transf.*, **22**, 1995, 212-219.

[19] Denier, J. P., Hewitt, R. E., Asymptotic matching constraints for a boundary-layer flow of a power-law fluid, *J. Fluid Mech.*, **518**, 2004, 261-279.

[20] Hossain, M. A., Grola, R. S.R., Natural convection flow of non-Newtonian power-law fluid from a slotted vertical isothermal surface, *Int. J. Numer. Method H.*, **19**, 2009, 835-846.

[21] Molla, M. M., Yao, L. S., The Flow of Non-Newtonian fluids on a flat plate with a uniform heat flux, *ASME J. Heat Transf.*, **131**, 2009, 1-6.

[22] Siddiqa, S., Begum, N., Hossain, M. A., Massarotti, N., Influence of thermal radiation on contaminated air and water flow past a vertical wavy frustum of a cone, *Int. Commun. Heat Mass Transf.*, **76**, 2016, 63-68.

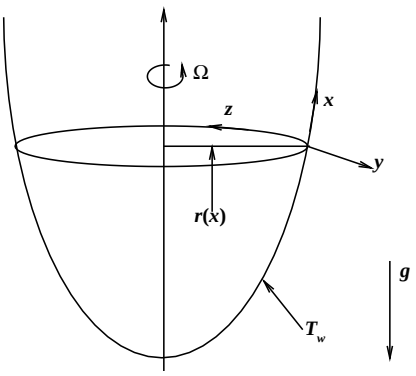

Fig. 1 Physical Model

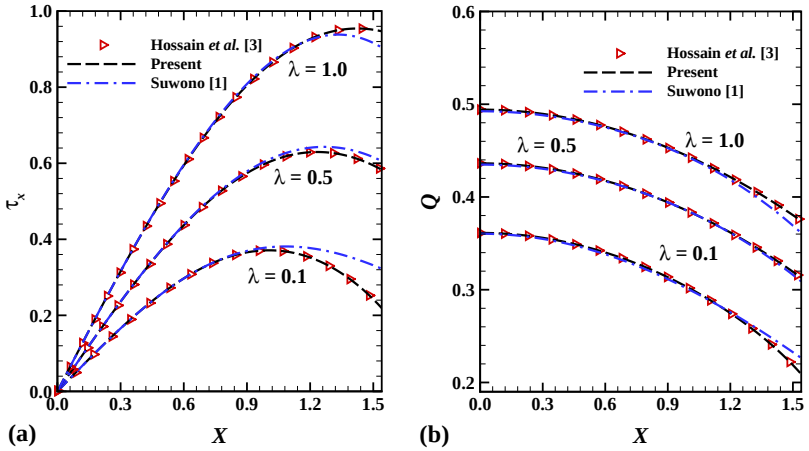

Fig. 2 (a) τ and (b) Q for $\lambda = 0.1, 0.5, 1.0$, $\mathbf{Pr} = 0.72$, $n = 1.0$.

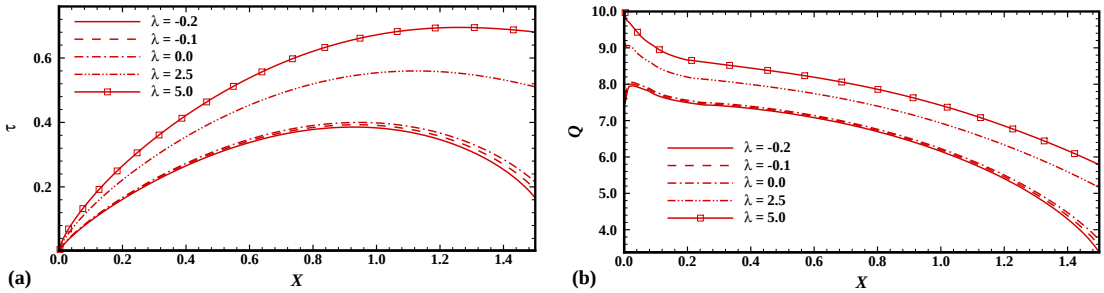

Fig. 3 (a) τ and (b) Q for $\lambda = -0.2, -0.1, 0.0, 2.5, 5.0$, $\mathbf{Pr} = 1000.0$, $n = 1.6$.

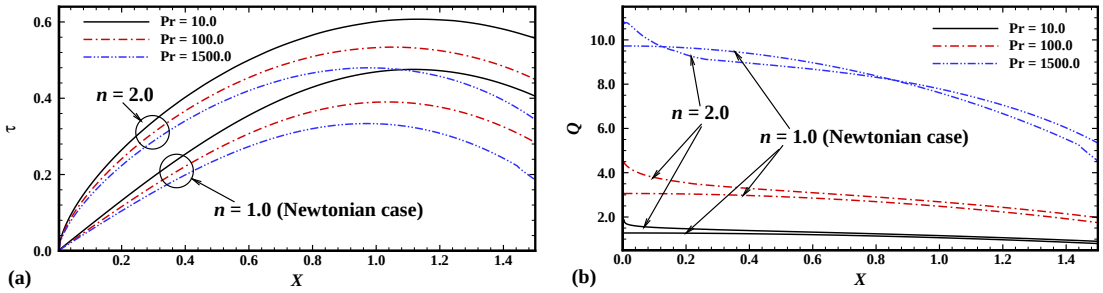

Fig. 4 (a) τ and (b) Q for Pr $= 10.0, 100.0, 1500.0$, $X = 1.0, 2.0$, $\lambda = 0.5$.

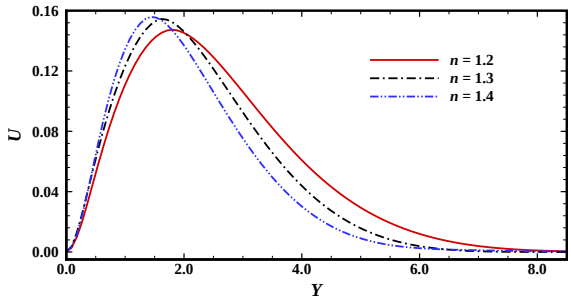

Fig. 5 Velocity profile for $n = 1.2, 1.3, 1.4$, $\lambda = -0.5$, Pr $= 1000.0$.

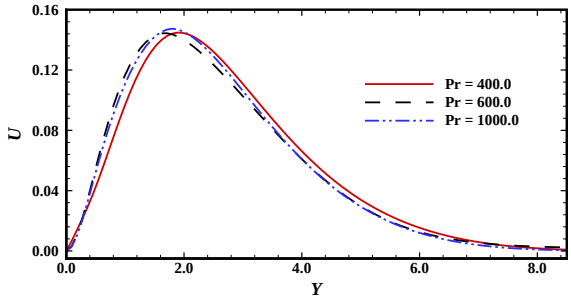

Fig. 6 Velocity profile for Pr $= 400.0, 600.0, 1000.0$, $n = 1.2$, $\lambda = -0.5$.

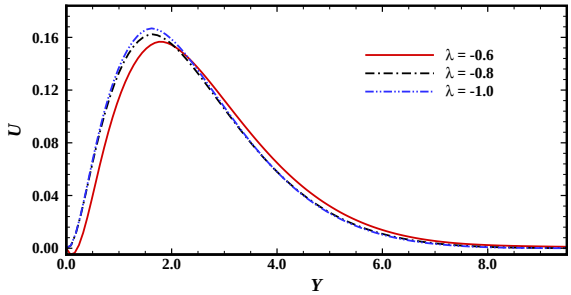

Fig. 7 Velocity profile for $\lambda = -0.6, -0.8, -1.0$, Pr $= 500.0$, $n = 1.2$.